Q. J. R. Meteorol. Soc. (2006), **132**, pp. 2333–2355 doi: 10.1256/qj.05.216

Microwave land emissivity and skin temperature for AMSU-A and -B assimilation over land

By FATIMA KARBOU*, ÉLISABETH GÉRARD and FLORENCE RABIER
CNRM/GAME, Météo-France/CNRS, Toulouse, France

(Received 31 October 2005; revised 25 May 2006)

SUMMARY

AMSU-A and -B measurements are still not extensively used over land surfaces for atmospheric applications. Recent studies have shown that it should now be possible to take advantage of the information content of these instruments provided land emissivity and skin temperature estimates are improved. This paper reports on comparisons between three land-surface schemes using the Météo-France four-dimensional variational (4D-Var) assimilation system. Firstly, a monthly mean estimated land emissivity atlas using AMSU data is used. A second land-surface scheme based on direct emissivity calculations is developed to obtain dynamically emissivity values. The third approach is based on the first one with the addition of a dynamic skin temperature estimation based on one AMSU-A or AMSU-B window channel. The land-surface schemes described above have been implemented within the 4D-Var system and their results have been compared with those of the operational surface scheme (which uses emissivity models). All land schemes have been evaluated by examining the performances of the observation operator for sounding channels prior to the assimilation. With dynamically varying emissivities and/or skin temperatures or with averaged emissivities, the simulations are clearly improved compared with the operational model and many more data pass the quality-control check.

KEYWORDS: Data assimilation Polar-orbiting satellite Sounders

1. INTRODUCTION

The Advanced Microwave Sounding Units (AMSU) A and B are carried by the latest generation of the National Oceanic and Atmospheric Administration (NOAA) polar-orbiting satellites. Similar sounders have recently been taken on board the National Aeronautics and Space Administration (NASA) Earth Science satellite mission Aqua (AMSU-A and Humidity Sensor for Brazil) and on board the NOAA 18 satellite (Microwave Humidity Sounder). AMSU-A and AMSU-B instruments have channels near the 50–60 GHz oxygen absorption band and near the 183.31 GHz water vapour absorption line respectively. In addition, both instruments make measurements at frequencies associated with rather high atmospheric transmission. Therefore, measurements obtained from these sounders can be used to obtain atmospheric temperature and humidity information and also to derive surface parameters over all surfaces. Given the inhomogeneous distribution of *in situ* measurements over oceans and over land, efforts are being made to extend the use of AMSU measurements in weather forecasting systems.

So far, the assimilation of AMSU observations has been preferentially developed for channels that are not sensitive to the surface. The assimilation of surface channels requires both accurate surface temperature and emissivity descriptions. These requirements are more easily satisfied over oceans than over land surfaces. Unlike oceans, land surfaces are associated with rather high emissivities (almost 1.0). In such cases, it is difficult to distinguish atmospheric and surface contributions. For many reasons this limitation is less important over the ocean. The ocean is characterized by lower emissivity values but also by higher emissivity polarization differences. Several ocean emissivity models have been developed (Rosenkranz and Staelin 1972; Wentz 1975; Guissard and Sobieski 1987; Prigent and Abba 1990; Guillou *et al.* 1998; Deblonde

* Corresponding author: 42 avenue de Coriolis, 31057 Toulouse, France. e-mail: fatima.karbou@cnrm.meteo.fr

and English 2000, among many others) that are accurate enough for use in atmospheric applications. However, the uncertainties of these models should not be ignored.

Over land, emissivity modelling has additional difficulties as emissivity varies in time and space and with surface types, roughness and moisture content.

Nevertheless, several studies have been carried out to overcome the modelling limitations (see for example Grody 1988; Isaacs *et al.* 1989; Weng *et al.* 2001). Their models require reliable input parameters (soil moisture, vegetation description, soil roughness, among others) to give emissivity estimates with an accuracy that meets the numerical weather prediction (NWP) requirements. On a global scale, these input parameters are still poorly described.

Besides emissivity modelling, several studies have been conducted to investigate emissivity variations with surface conditions. For instance, ground-based microwave measurements have been used by Mätzler (1990, 1994), Calvet *et al.* (1995) and Wigneron *et al.* (1997) to characterize the emissivity over different surface types. Hewison and English (1999) and Hewison (2001) estimated forest, agricultural, snow and ice emissivities with airborne high-frequency radiometers. Satellite measurements have also been used to estimate land-surface emissivities. Felde and Pickle (1995) used data from the Special Sensor Microwave/Temperature-2 (SSM/T2) instrument to retrieve surface emissivities at 91 and 150 GHz. Choudhury (1993) estimated surface reflectivity using the Special Sensor Microwave/Imager (SSM/I) measurements at 19 and 37 GHz. Jones and Vonder Haar (1997) and Morland *et al.* (2000, 2001) among others, computed surface emissivities based on different microwave satellite data. Prigent *et al.* (1997, 1998) used SSM/I measurements in order to derive emissivities at frequencies ranging from 19 to 85 GHz. SSM/I emissivities have been used to model emissivities at AMSU-A frequencies and scanning conditions (Prigent *et al.* 2000). With a view to retrieving atmospheric humidity and temperature, Karbou *et al.* (2005a) used measurements from AMSU-A and -B to calculate emissivities at frequencies ranging from 23 to 150 GHz and at observation zenith angles up to 58°. Analyses of angular and frequency dependencies of AMSU emissivities show that it is possible to derive emissivity parametrization based on AMSU emissivity estimates to help process AMSU measurements over land (Karbou 2005).

At present, the assimilation of AMSU observations is restricted to mid- and upper-tropospheric sounding channels. Recent developments have shown that it is now possible to estimate emissivity at AMSU surface channels with an error of 2% at a range of frequencies and scanning angles (Karbou *et al.* 2005a). Such emissivity estimates combined with accurate skin temperatures have been found useful for extracting atmospheric information over land using neural network methods (Karbou *et al.* 2005b). English (1999), who studied the role of emissivity and skin temperature in the context of variational retrievals over land, came to similar conclusions. Direct emissivity calculations have been performed within the 4D-Var system of the European Centre for Medium-range Weather Forecasts (ECMWF) to prepare AMSU-A assimilation over land (Prigent *et al.* 2005).

The studies mentioned above show that useful atmospheric information from AMSU sensors or equivalent instruments can be extracted over land with the help of improved emissivity and skin temperature estimates. The purpose of this paper is to investigate the impact of an improved microwave emissivity and/or skin temperature within the framework of operational assimilation. This study is a preparatory step in order to extend the still-restricted use of AMSU-A and -B channels over land in NWP models. The paper is organized as follows. The AMSU observations and emissivity datasets are described in section 2. Three land-surface schemes are presented in

TABLE 1. AMSU-A AND -B CHARACTERISTICS AND CONDITIONS FOR USE

Channel	Frequency (GHz)	Noise equivalent (K)	Conditions for use
AMSU-A			
1	23.8	0.20	Not used
2	31.4	0.27	Not used
3	50.3	0.22	Not used
4	52.8	0.15	Not used
5	53.596 ± 0.115	0.15	Clear sky, open sea, land with orog. <500 m
6	54.4	0.13	Clear sky, open sea, land with orog. <1500 m
7	54.9	0.14	Not used if (cloudy, $\|\text{lat}\| \leq 30°$)
8	55.5	0.14	Not used if (cloudy, $\|\text{lat}\| \leq 30°$)
9	$57.290 (= \nu_9)$	0.20	Used
10	$\nu_9 \pm 0.217$	0.22	Used
11	$\nu_9 \pm 0.322 \pm 0.048$	0.24	Used
12	$\nu_9 \pm 0.322 \pm 0.022$	0.35	Used
13	$\nu_9 \pm 0.322 \pm 0.010$	0.47	Not used
14	$\nu_9 \pm 0.322 \pm 0.0045$	0.78	Not used
15	89	0.11	Not used
AMSU-B			
1	89	0.37	Not used
2	150	0.84	Not used
3	183 ± 1	0.60	Sea, clear sky
4	183 ± 3	1.06	Sea, land and orog. <1500 m, clear sky
5	183 ± 7	0.70	Sea, land and orog. <1000 m, clear sky

section 3. Within these schemes, the emissivity and/or skin temperature are updated. The results are discussed and compared with the control land scheme (operational model) in section 4. Section 5 concludes this study.

2. DATA AND METHOD

(*a*) *AMSU data*

The AMSU-A sensor makes measurements in 15 frequencies ranging from 23.8 to 89 GHz. The sounding channels near the oxygen absorption band (50–60 GHz) are used to estimate tropospheric and stratospheric temperatures. AMSU-A has two separate units: the first one (AMSU-A1) gives measurements at 12 frequencies within the 50–60 GHz band and at 89 GHz. Two antennae are integrated into this unit. The second one (AMSU-A2) makes measurements at 23.8 and 31.4 GHz.

AMSU-B is designed for tropospheric humidity retrievals with the help of three channels centred on the 183.31 GHz water vapour line. The instrument has two other channels at 89 and 150 GHz, mainly sensitive to surface and to low atmospheric layers.

AMSU A and B sample 30 and 90 Earth views with a nominal field of view of 3.3° and 1.1°, respectively. As a consequence, the AMSU observation scan angle varies from −48° to +48° which translates into ±58° zenith angle variation. Table 1 lists frequency characteristics of AMSU sensors. Further details about these instruments can be found in Goodrum *et al.* (2000).

(*b*) *Emissivities from AMSU measurements*

To calculate emissivities from satellite observations, the surface is usually assumed to be flat and specular. This assumption, useful when no a priori information about

the surface is available, has been adopted by several authors (Jones and Vander Haar 1997; Prigent *et al.* 1997; Weng *et al.* 2001; Karbou *et al.* 2005a, among others). Mätzler (2005) suggests that the use of this approximation for nadir-viewing sensors is questionable because the Lambertian component can be significant in very specific cases (for example, over some metallic surfaces). Karbou and Prigent (2005) have shown that the impact of the specular assumption on the retrieved near-nadir AMSU emissivities when the surface is Lambertian is well below 1% of emissivity bias in most atmospheric situations over natural snow-free areas. The use of a specularity parameter, as suggested by Mätzler (2005), could probably reduce the already small effect of the specular assumption. Nevertheless, such a parameter is difficult to assess in the framework of global applications.

For a non-scattering plane-parallel atmosphere and for a given AMSU path zenith angle and frequency, the brightness temperature, T_b, observed by the sensor can be expressed as

$$\left.\begin{aligned} T_b(\nu,\theta) &= T_s\varepsilon(\nu,\theta)\Gamma + \{1-\varepsilon(\nu,\theta)\}\Gamma T_a^{\downarrow}(\nu,\theta) + T_a^{\uparrow}(\nu,\theta) \\ \Gamma &= \exp\left\{\frac{-\tau(0,H)}{\cos\theta}\right\}, \end{aligned}\right\} \tag{1}$$

where $T_b(\nu,\theta)$ and $\varepsilon(\nu,\theta)$ represent the T_b measured by the sensor and the surface emissivity, respectively, at frequency ν and at observation zenith angle θ. T_s, $T_a^{\downarrow}(\nu,\theta)$, and $T_a^{\uparrow}(\nu,\theta)$ are the skin temperature, the atmospheric downwelling and upwelling T_bs, respectively. Γ is the net atmospheric transmissivity and can be expressed as a function of the atmospheric opacity $\tau(0,H)$ and the observation zenith angle θ. H is the top-of-atmosphere height.

The microwave land emissivity can then be retrieved from

$$\varepsilon(\nu,\theta) = \frac{T_b(\nu,\theta) - T_a^{\uparrow}(\nu,\theta) - T_a^{\downarrow}(\nu,\theta)\Gamma}{\{T_s - T_a^{\downarrow}(\nu,\theta)\}\Gamma}. \tag{2}$$

AMSU measurements are made with a system of rotating antennae. As a consequence, the calculated emissivities are a mixture between emissivities in the vertical and the horizontal polarizations. Under the assumption of a nominal performance of the AMSU instrument, this relationship could be expressed by

$$\left.\begin{aligned} \varepsilon(\nu,\theta) &= \varepsilon_p(\nu,\theta)\cos^2\varphi + \varepsilon_q(\nu,\theta)\sin^2\varphi, \\ \varphi &= \arcsin\left(\frac{R}{R+H_{sat}}\sin\theta\right). \end{aligned}\right\} \tag{3}$$

Here, θ and φ are the satellite zenith and scan angles respectively. φ can be expressed as a function of the observation zenith angle θ, the radius of the Earth R and the satellite height H_{sat}.

$\varepsilon_p(\nu,\theta)$ and $\varepsilon_q(\nu,\theta)$ are emissivities at the two orthogonal polarizations. For AMSU window channels, the polarization is assumed to be vertical at nadir. Consequently, Eq. (3) translates into

$$\varepsilon(\nu,\theta) = \varepsilon_v(\nu,\theta)\cos^2\varphi + \varepsilon_h(\nu,\theta)\sin^2\varphi. \tag{4}$$

Here, $\varepsilon_v(\nu,\theta)$ and $\varepsilon_h(\nu,\theta)$ are emissivities at the vertical and horizontal polarizations respectively.

3. The assimilation system and three surface configurations for AMSU radiance computation

(*a*) *The assimilation system*

Given a set of observations and background information (short-range forecast from a previous analysis), a 4D-Var system finds the model solution that represents the optimal balance between all available information. If we assume that observations and background errors are uncorrelated and have Gaussian distributions, then the 4D-Var solution $\mathbf{x}$ (state of atmosphere) is obtained by minimizing a cost function $J(\mathbf{x})$ given by

$$J(\mathbf{x}) = \frac{1}{2}(\mathbf{x}-\mathbf{x}^{\mathrm{b}})^{\mathrm{T}}\mathbf{B}^{-1}(\mathbf{x}-\mathbf{x}^{\mathrm{b}}) + \frac{1}{2}\sum_{i=0}^{N}\{\mathcal{H}_i(\mathbf{x}_i)-\mathbf{y}_i^{\mathrm{o}}\}^{\mathrm{T}}\,\mathbf{R}_i^{-1}\{\mathcal{H}_i(\mathbf{x}_i)-\mathbf{y}_i^{\mathrm{o}}\}, \qquad (5)$$

where $\mathbf{x}$ is the model state at time t_0; $\mathbf{x}^{\mathrm{b}}$ is the background state at time t_0; $\mathbf{B}$ is the background-error covariance matrix of $\mathbf{x}^{\mathrm{b}}$; $\mathbf{y}_i^{\mathrm{o}}$ is the observation vector at time t_i; $\mathcal{H}_i$ is the observation model operator at time t_i; $\mathbf{R}_i$ is the observation-error covariance matrix at time t_i (including $\mathcal{H}_i$ errors); $\mathbf{x}_i$ is the model state at time t_i, and subscripts $^{-1}$ and $^{\mathrm{T}}$ indicate the matrix inverse and transpose, respectively.

This paper relies on the Météo-France assimilation and forecast model system (ARPEGE) that uses a 6-hour time window and a multi-incremental 4D-Var (Courtier *et al.* 1994; Veersé and Thépaut 1998; Rabier *et al.* 2000). The minimization of Eq. (5) is performed in two steps, with simplified and with more complete physics, respectively (Janiskova *et al.* 1999). For satellite radiance assimilation, $\mathcal{H}_i(\mathbf{x}_i)$ is a radiative transfer model that provides model equivalents to the satellite radiance. In our case, we used the RTTOV model (Radiative Transfer for the Television and Infrared Observation Satellite (TIROS) Operational Vertical sounder; Eyre 1991; Saunders *et al.* 1999, Matricardi *et al.* 2004). Model equivalent computations are performed once surface emissivity and bias-correction coefficients (among other parameters) are defined. Then, short-range forecast data (temperature/humidity profiles and surface temperature) are used as inputs to the radiative transfer model.

As explained above, our main objective is to investigate the use of alternatives to the operational microwave emissivity and/or skin temperature within the framework of NWP data assimilation. In this paper, we examine the impact on the observation-operator simulations. Emissivity models (currently used in the operational system) facilitate the assimilation of channels that receive a weak contribution from the surface. However, these models are not yet accurate enough to allow the assimilation of surface-sensitive channels. (See Table 1 for the current use of AMSU-A & -B channels in the 4D-Var system). Currently, depending on surface type and observation frequency, the Météo-France 4D-Var system uses Grody (1988) or Weng *et al.* (2001) models to get emissivity estimates at AMSU frequencies. Figures 1(a) and (b) show mean emissivity maps averaged over a two-week period (from 22 March to 4 April 2005) and obtained at 23.8 and 89 GHz using the operational surface scheme. In this study, our goal is to improve the AMSU observation operator simulations over land, which requires that the surface (emissivity and/or skin temperature) is better described.

To reach our objective, three alternative land-surface schemes are tested. All schemes are designed to be easily handled by the observation operator and more specifically by the RTTOV model.

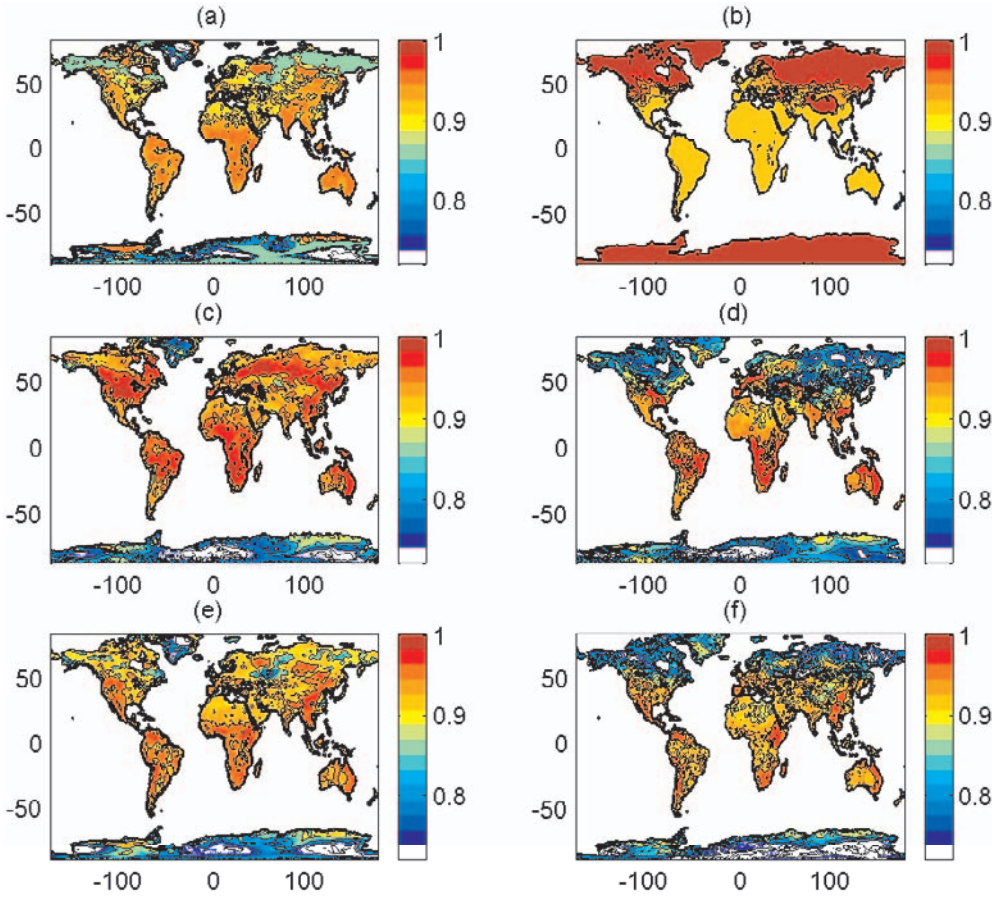

Figure 1. Mean emissivity maps averaged over a two-week period and obtained with the operational surface scheme at (a) 23.8 GHz and (b) 89 GHz. (c) and (d) are as (a) and (b) but with the first land-surface scheme (using an emissivity atlas from year 2000). (e) and (f) are as (a) and (b) but with the second land-surface scheme.

(*b*) *Monthly mean emissivity atlases*

Cloud-free observations from year 2000 have previously been used to estimate land emissivities at AMSU surface channels (23.8, 31.4, 50.3, 89, and 150 GHz) and for different observation zenith angles (from $-58°$ to $58°$). Cloud screening has been performed using collocated visible/infrared satellite measurements from the International Satellite Cloud Climatology Project (ISCCP; Rossow and Shiffer 1991). The ISCCP database also provides accurate skin temperature estimates. The corresponding temperature and humidity profiles from the ECMWF 45-year re-analysis (ERA-40; Simmons and Gibson 2000; Uppala *et al.* 2005) have been used as input to a state-of-the-art microwave radiative transfer model (Pardo *et al.* 2001) in order to estimate the atmospheric contribution to the measured radiance.

The emissivities thus obtained have been analysed and their angular and frequency dependencies inspected. The analysis shows that it is possible to extrapolate the emissivity at sounding frequencies from the window channel estimates. The temporal and spatial variations of AMSU emissivities have also been studied. In addition, good agreement has been found in comparison between AMSU and SSM/I emissivities (from

Prigent *et al.* 1997). More details about AMSU emissivity estimation and analysis can be found in Karbou *et al.* (2005a).

The first configuration uses a monthly mean land emissivity atlas based on February 2000 AMSU-A and -B near-nadir observations to get updated emissivity values at 23.8, 31.4, 50.3, 89, and 150 GHz. Emissivity estimates obtained at window channels have been used for the closest sounding channels without extrapolation. For instance, emissivity at 50.3 GHz is used for the 51–60 GHz channels. Figures 1(c) and (d) show mean February emissivity maps at 23.8 and 89 GHz. The experiment conducted with this land configuration is noted as Exp1–Atlas2000 below. It should be noted that the emissivity atlas for year 2000 was obtained with NOAA-15 AMSU data. The use of an emissivity atlas based on additional instruments and on a period closer to the experiment period is preferable. Therefore, another experiment has been conducted using a similar emissivity atlas obtained during the first 20 days of March 2005 (following the methodology of section 2(b)). The experiment conducted with this land configuration is noted as Exp1–Atlas2005 below.

(*c*) *Dynamic emissivity calculations*

New emissivity calculations following the methodology described in section 2(b) have been conducted over a two-week period (22 March to 4 April 2005) within the Météo-France 4D-Var assimilation system. The atmospheric components have been computed using the RTTOV model.

In the framework of operational assimilation, an a priori knowledge of cloud contamination is difficult to obtain. Moreover, for the new emissivity computations and in order to meet the constraints of operational assimilation, no cloud clearing has been attempted. Cloudy situations are rejected in the quality-check step where only relatively small differences between observations and simulations are tolerated. New emissivities are calculated for each atmospheric situation and at 23.8 GHz (AMSU-A channel 1) and at 89 GHz (AMSU-B channel 1). These emissivities are then allocated to higher AMSU-A and AMSU-B frequency channels, respectively, without extrapolation. Previous analyses have revealed that, for most surfaces, AMSU emissivities vary smoothly with frequency and that it is possible to use window frequency emissivities for sounding ones (Karbou *et al.* 2005a). The smooth emissivity variation with frequency has been also observed by Choudhury (1993), Jones and Vonder Haar (1997), and Prigent *et al.* (1997, 2000), among others.

These dynamic emissivities are supplied within the second surface scheme (noted Exp2 hereafter). Figure 1 compares emissivities at 23.8 and 89 GHz averaged over the same two-week period as obtained using the operational, the first (with Atlas2000), and the second surface configurations. This figure shows that the calculated emissivities (from Exp1–Atlas2000 and Exp2) exhibit spatial structures that are compatible with surface type. For instance, lakes and rivers are associated with lower emissivities (the Amazon river and some lakes in Africa can be easily recognized). Emissivities calculated at 89 GHz (Figs. 1(d) and (f)) show expected changes with surface type and give more detailed emissivity variations than those obtained with the operational surface scheme (see Fig. 1(b)). Even if a perfect emissivity model existed, the quality of its outputs would highly depend on its input parameters. Being calculated using different periods, it is quite difficult to compare Exp1–Atlas2000 emissivities with the newly calculated ones. However, emissivity histograms show that both datasets have similar distributions and that they differ from the histogram of emissivities coming from the operational surface scheme. Figure 2 shows histograms of emissivities at 23.8 and at 89 GHz calculated globally. The peak-like features of the operational (control) surface

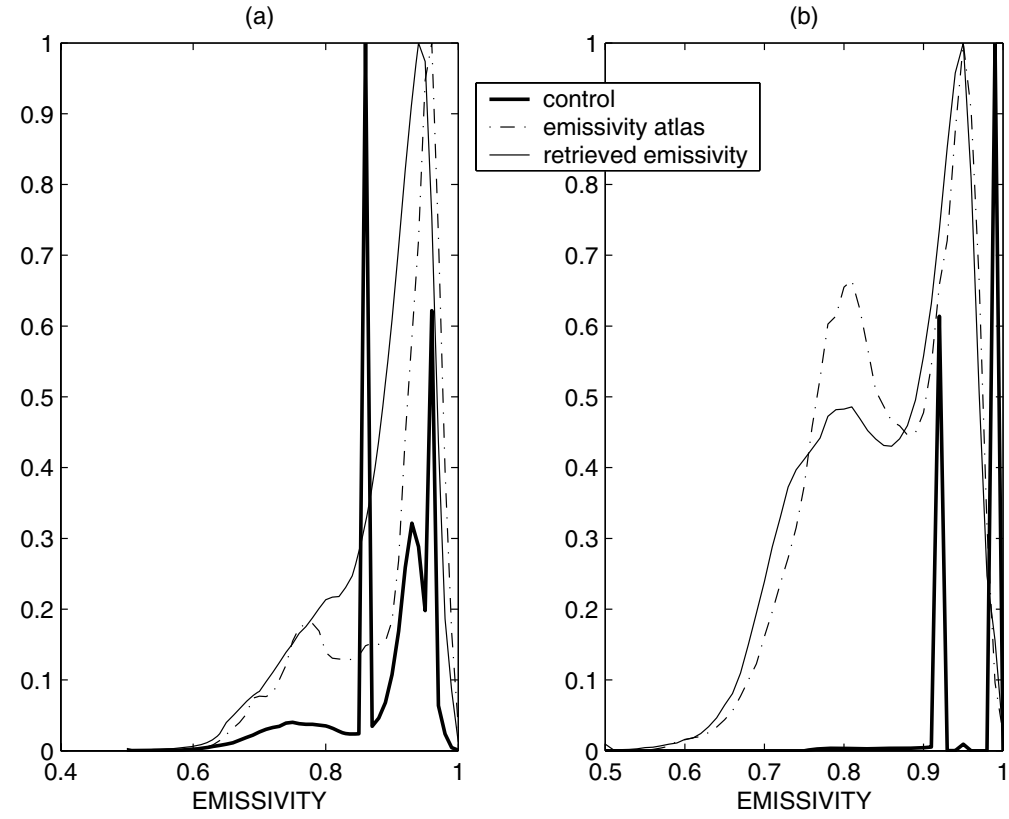

Figure 2. Emissivity histograms computed globally from the control (bold solid), from Exp1 (dash-dotted) and from Exp2 (thin solid), at (a) 23.8 GHz and (b) 89 GHz.

scheme emissivity histograms are due to constant emissivity values attributed to some surface types (snow, sea-ice, etc.)

Direct emissivity measurements are lacking but are badly needed for evaluation of emissivity datasets. However, the evaluation of the emissivity estimation procedure could be done using ocean data. For this purpose, emissivities at 23.8 GHz computed using a fast sea emissivity model (Deblonde and English 2000) have been compared with the ones obtained with Eq. (2). Using the equation, we do expect higher errors over ocean than over land. Indeed, emissivities over the ocean are generally within 0.4–0.5 against 0.95–1.0 over land. If we assume that the absolute error of the computed emissivities is within 2% over land, then relative emissivity error over land and ocean should be near 2% and 4% respectively. In spite of this limitation, rather good agreement has been observed between the two emissivity datasets (not shown). In section 4, indirect evaluations will be carried out by comparing simulated (with all land-surface configurations) and observed brightness temperatures.

(*d*) *Monthly mean emissivity atlases and dynamic skin temperature estimation*

Accurate skin temperatures as well as land emissivities are required for NWP applications over land. At some frequencies, microwave measurements are very sensitive to the surface and are less affected by non-precipitating clouds than are infrared observations. Therefore, microwave measurements can potentially provide better skin

temperature estimates than the infrared in different atmospheric situations. Assuming that surface air and skin temperature variations are similar, several methods have been developed to estimate near-surface temperature over land using SSM/I observations (see for instance MacFarland *et al.* 1990; Basist *et al.* 1998; Williams *et al.* 2000). This assumption is not strictly valid because the diurnal and seasonal cycles of skin temperature (as well as variations at longer time-scales) differ from those of air temperature. Neural network methods have also been used to estimate skin temperatures together with other surface variables from SSM/I and infrared observations (Aires *et al.* 2001; Prigent *et al.* 2003). Trigo and Viterbo (2003) illustrate how errors in skin temperature can restrict the assimilation of channels from polar-orbiting sounders.

In the third land configuration, we derive skin temperature estimates from AMSU-A or AMSU-B observations that will be used with the previously calculated emissivity atlases. For this task, a physical method is employed using one AMSU-A channel (or one AMSU-B channel) and a precalculated mean emissivity atlas. The calculated skin temperature is used as a guess for the remaining channels during the observation operator simulations (it replaces the background surface temperature). The channel used for skin temperature computation will not be assimilated. The surface temperature will be analysed afterwards as is the case in the operational model.

However, skin temperature is quite difficult to define because the penetration depth is not the same from one channel to another. Consequently, the skin temperature calculated at any one frequency may not be adapted for use at other frequencies. Moreover, errors in the mean emissivity atlases will contribute to biases in skin temperature estimates.

At a selected frequency ν_1, the skin temperature can be derived from Eq. (1) as

$$T_s = \frac{T_b(\nu_1, \theta) - (1 - \varepsilon_{atlas}) T_a^{\downarrow}(\nu_1, \theta)\Gamma - T_a^{\uparrow}(\nu_1, \theta)}{\varepsilon_{atlas}\Gamma}. \tag{6}$$

Here, ε_{atlas} represents the monthly mean emissivity atlas.

Before using the method, we evaluated it using a one-month period in the year 2000. For this evaluation, AMSU data from July 2000 have been used to derive skin temperatures at four AMSU-A channels (23.8, 31.4, 50.3, and 89 GHz) and over large areas (60°E–60°W; 60°S–60°N). Computations were performed using a mean emissivity atlas at 23.8 GHz from February 2000. The skin temperatures thus obtained were then compared with the ISCCP ones. Figure 3 shows scatter plots for July 2000 ISCCP skin temperatures versus estimated skin temperatures at AMSU surface channels. We notice a rather good agreement between the estimated AMSU skin temperatures and the target ones, especially at low frequencies. At 89 GHz, the agreement is less good. This can be explained by the increase of the sensitivity to errors in the atmosphere with higher frequencies. Moreover, the use of a winter emissivity atlas (here February data) is not optimal to compute summer skin temperatures. A good agreement is also found between skin temperatures estimated at the four AMSU frequencies (23.8, 31.4, 50, and 89 GHz). The differences between computed skin temperatures could be due to atmospheric, cloud contamination, and emissivity atlas errors, among other reasons.

Nevertheless, the skin temperature difference histograms (not shown) show that skin temperature can be estimated from AMSU surface channels within 5 K of standard deviation over a variety of surface types. It is worth mentioning that the ISCCP land skin temperature accuracy is assumed to be within 4 K, as reported by Rossow and Garder (1993a,b).

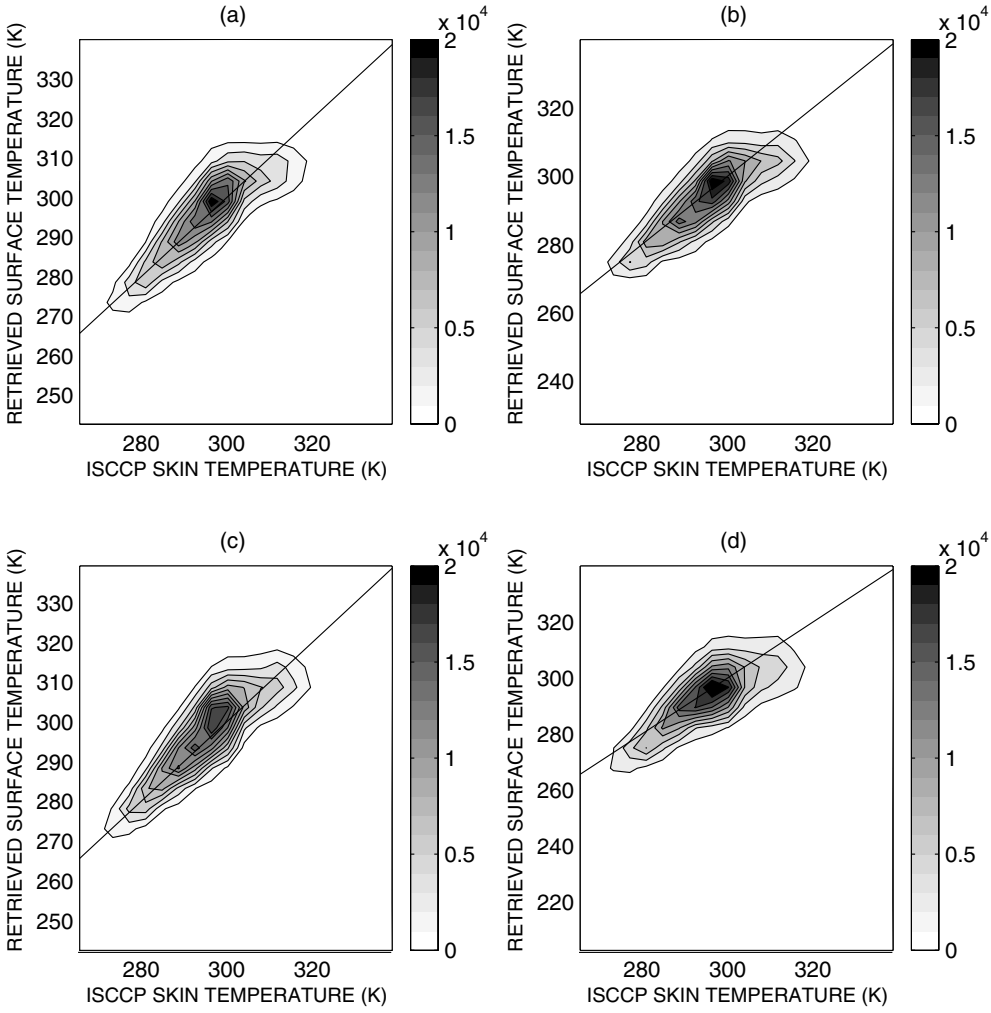

Figure 3. Scatter plots of July 2000 ISCCP skin temperature versus estimated skin temperature using frequencies (a) 23.8 GHz, (b) 31.4 GHz, (c) 50.3 GHz, and (d) 89 GHz. The grey shading indicates the number of observations.

Figure 4 compares surface temperatures from two weeks of the operational system background, with the retrieved skin temperatures using AMSU-A channel 1. The retrieved skin temperatures show a more detailed spatial variation than the background surface temperatures. The histogram of the retrieved skin temperatures (not shown) differs from that of the surface temperatures. The retrieved skin temperatures will be indirectly evaluated by comparing simulated and observed brightness temperatures. These developments constitute our third land-surface scheme (noted below as Exp3).

4. Result comparisons

(*a*) *Sensitivity of brightness temperatures to emissivity and/or skin temperature errors*

In order to compute emissivity estimates, we make use of several ancillary pieces of information. As a consequence, emissivity accuracy depends on errors in the input

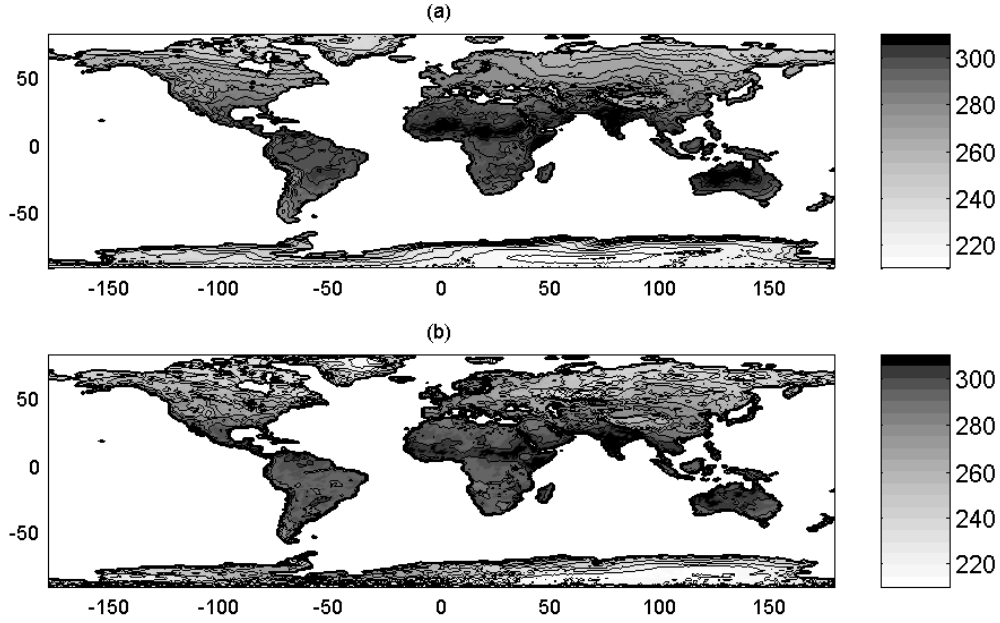

Figure 4. Mean surface temperatures (K) averaged over a two-week period obtained from (a) the operational system background and from (b) the retrieved skin temperatures at AMSU-A channel 1.

parameters. The sensitivity of emissivity to various input errors has been previously studied (Karbou *et al.* 2005a). The accuracy of calculated land-surface emissivity using satellite observations has been evaluated by analysing the change in the emissivity due to a variation in one of the input parameters, with the others remaining unchanged. Thus, the impacts of an alteration of $\pm 15\%$ in humidity profile, ± 1 K in temperature profile, ± 4 K in skin temperature, and ± 1 K in brightness temperature have been studied. This analysis has been performed using 5 days from early January 2000 and for frequencies ranging from 23 to 150 GHz. The emissivity variations have been examined by separating low- and high-zenith-angle observations, as well as dry and very moist atmospheric conditions. It was found that, for all AMSU channels, the accuracy of the estimated emissivities is degraded in cases of high zenith angles and very moist conditions. For such cases, the atmospheric transmission decreases as well as the sensitivity to the surface. Errors in the humidity profiles are found to have great effects at 89 and 150 GHz and a lesser effect on the surface channels 23.8, 31.4 and 50.3 GHz (less than 0.25% of relative error). Errors in skin temperatures greatly influence the estimated emissivity at all frequencies (up to 3% of emissivity errors with ± 4 K of skin temperature variations). As expected, errors in the air temperature profile produce larger emissivity variations at 50 GHz than at other frequencies that are located farther away from the oxygen absorption bands.

Emissivities calculated for the year 2000 are cloud-free and benefit from accurate skin temperature estimates (from ISCCP). The day-to-day variability of the calculated emissivities is found to be within 2% for all surface channels and for up to 45° observation zenith angle. We expect a degraded emissivity accuracy when emissivities are calculated using ancillary data from the 4D-Var background fields (Exp2). The operational system surface temperatures are less precise than the skin temperatures coming from ISCCP and no cloud-clearing is performed. Moreover, emissivities are only calculated

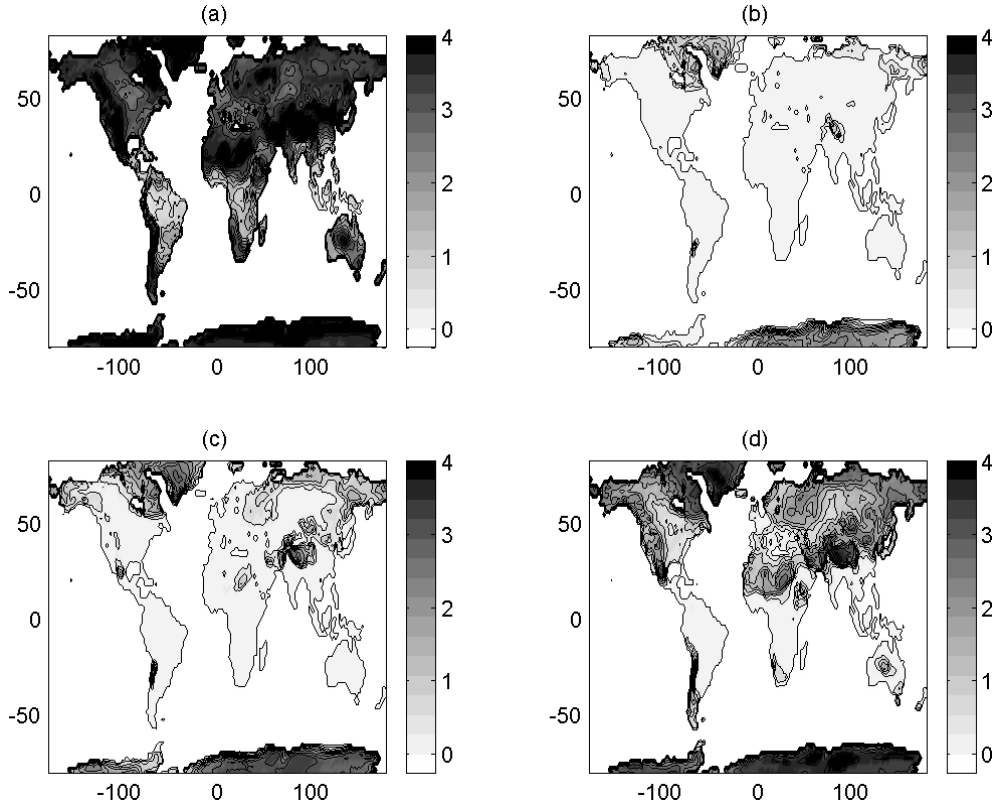

Figure 5. Mean brightness temperature variations (K) averaged over 2 days of data and obtained by introducing a 5 K skin temperature change. Results are shown for AMSU-B channels (a) 2, (b) 3, (c) 4, and (d) 5.

at 23.8 GHz and at 89 GHz (for AMSU-A and AMSU-B processing respectively) and are allocated to the remaining frequencies.

For skin temperature computation, errors from input parameters (background fields, emissivities from previously calculated atlases) will certainly degrade its accuracy. In section 2(d), we show that, despite all these limitations, we can expect a skin temperature accuracy of about 5 K in snow-free areas. In the context of operational assimilation, we used 2 days of AMSU data to evaluate the impact of an emissivity or a skin temperature variation on the simulated T_b. The T_b variation induced by an emissivity change, $\delta\varepsilon$, can be derived from Eq. (1) and expressed as

$$\delta T_{b,\delta\varepsilon} = \Gamma(T_s - T_a^{\downarrow})\delta\varepsilon. \tag{7}$$

In the same manner, T_b variation induced by a skin temperature change can be derived from Eq. (1),

$$\delta T_{b,\delta T s} = \Gamma\varepsilon\delta T_s. \tag{8}$$

Equations (7) and (8) are then used to estimate T_b variations if the variation of emissivity is equal to 0.02 and if the variation of skin temperature is equal to 5 K, for all AMSU-A and AMSU-B channels.

Figure 5 shows results for $\delta T_{b,\delta T s}$ using AMSU-B channels 2–5. $\delta T_{b,\delta T s}$ is mostly driven by the atmospheric transmission. AMSU-B channel 2 is associated with low atmospheric transmission in the tropics (more humidity in the atmosphere) and higher

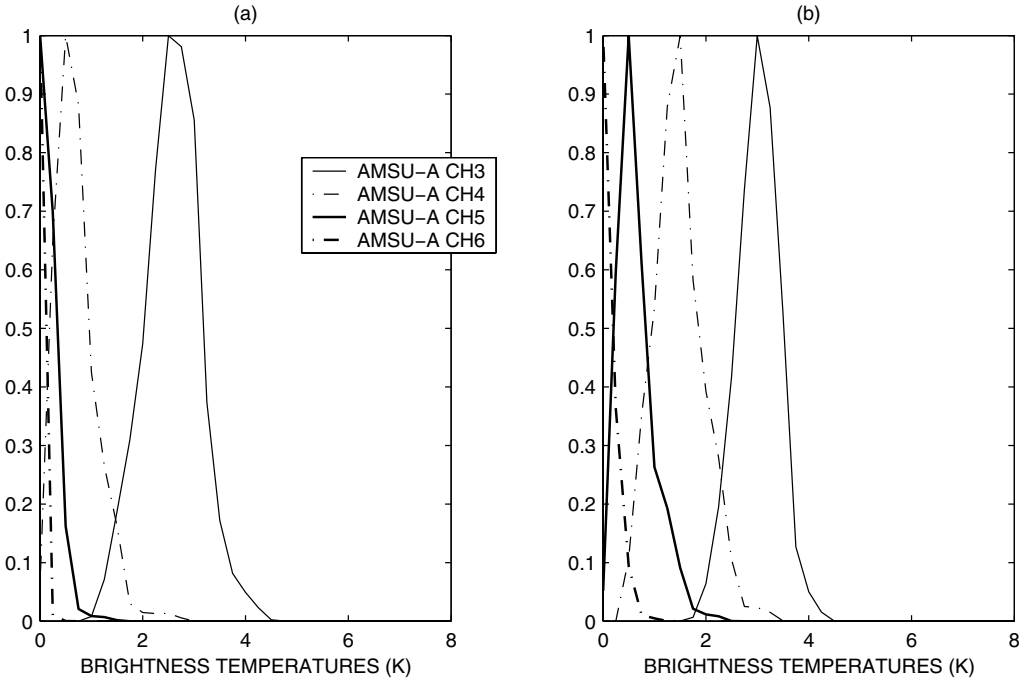

Figure 6. Histograms of brightness temperature variation for AMSU-A channels 3–6 induced by (a) a 2% emissivity change and (b) a 5 K variation in skin temperature.

ones in high-latitude areas. Figure 5(a) shows the expected variation of T_b for this channel. The other AMSU-B channels are associated with much lower transmission and the corresponding $\delta T_{b,\delta Ts}$ show maximum values over high-transmission areas (desert and Antarctica for channel 5, for example).

For AMSU-A channels (see $\delta T_{b,\delta\varepsilon}$ and $\delta T_{b,\delta Ts}$ histograms in Fig. 6), $\delta T_{b,\delta Ts}$ decreases with decreasing sensitivity to the surface. Mean $\delta T_{b,\delta Ts}$ values are found to be within 3, 1 and 0.5 K for AMSU-A channels 3, 4, and 5, respectively. On the other hand, a 2% emissivity variation modifies the AMSU T_b differently. Depending on the surface and the atmospheric conditions, this effect can be significant for surface channels but limited for channels less sensitive to the surface.

The computation of $\delta T_{b,\delta\varepsilon}$ and $\delta T_{b,\delta Ts}$ is strictly qualitative since we ignore errors coming from other input parameters. These computations only identify cases (channels, surface and atmospheric conditions) for which errors in emissivity and/or skin temperature impact significantly on the T_b simulations.

(*b*) *Brightness temperature computation using different land schemes*

The three land-surface schemes described above have been implemented within the 4D-Var system and their results have been compared with those obtained using the operational model. Therefore, a total of five experiments have been run covering the period 22 March to 4 April 2005 (Exp1–Atlas2000, Exp1–Atlas2005, Exp2, Exp3 and the control). In addition to AMSU observations, the control experiment (with the operational surface configuration) and the four other experiments make use of additional satellite, radiosonde, airborne and other conventional observations in the operational database.

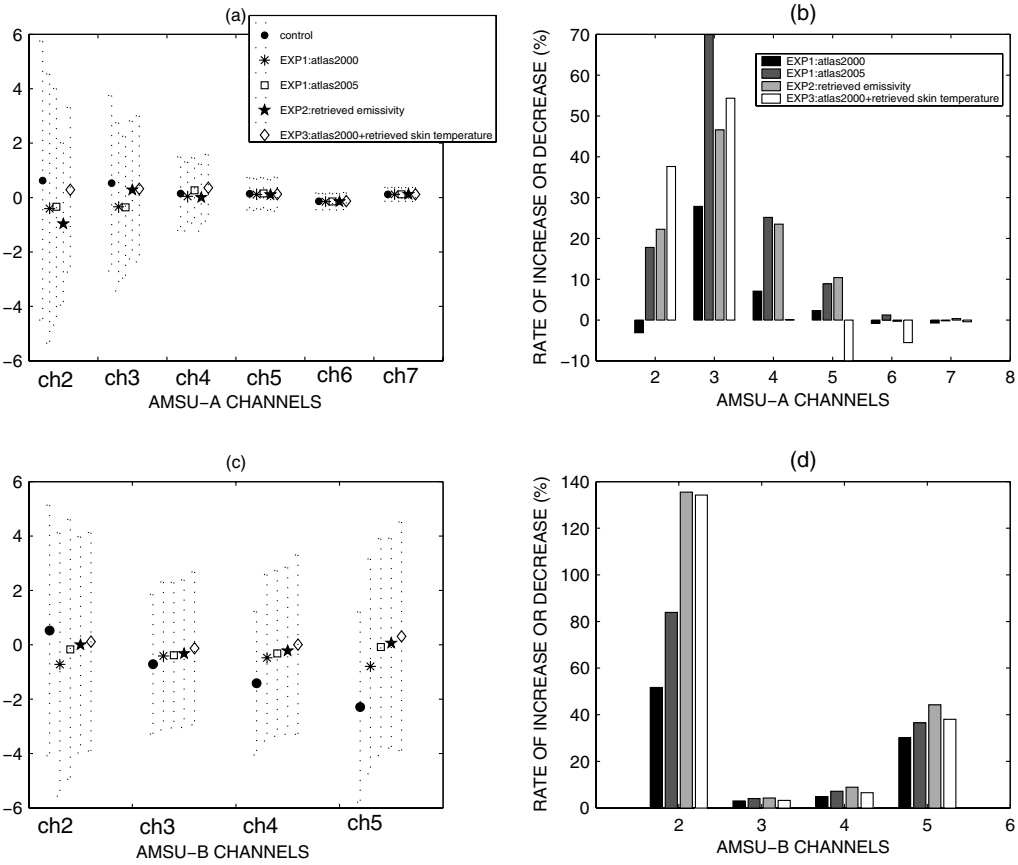

Figure 7. Global statistics from the five experiments: (a) mean fg-departures obtained for AMSU-A channels 2–7. Circle, asterisk, square, star, and diamond symbols give results from the control, the Exp1–Atlas2000, Exp1–Atlas2005, Exp2, and Exp3, respectively (see text for abbreviations), with fg-departure standard deviations, shown as dotted error-bars; (b) Rate of increase or decrease of the number of data within the range (−threshold⇒+threshold) with respect to the control experiment for AMSU-A channels 2–7. Here, the threshold is equal to 10, 6, 2.6, 1.2, 0.6, 0.6, respectively, for the six channels. (c) is as (a) but for AMSU-B channels 2–5. (d) is as (b) but for AMSU-B channels 2–5, with thresholds equal to 10, 8, 9, and 10, respectively, for the four channels.

To compare our five experiments, we compute for each one the differences between observed and simulated radiance using the background fields (called 'fg-departures' hereafter). The background field is used as a first guess, as is common practice in data assimilation. No bias corrections have been applied for these comparisons. Global statistics of fg-departures for all experiments, over the two-week period and for a selection of AMSU-A and -B channels (with a threshold defined for each channel), are presented in Fig. 7. For each experiment and for each channel, mean values, standard deviations (st.dev.) (Figs. 7(a) and (c)) and number of observations of fg-departures that are within the range (−threshold⇒+threshold) are computed. For experiments using updated surface configurations, a rate of increase or decrease of the number of observations with respect to the control experiment is also calculated (Figs. 7(b) and (d)).

Thresholds given in the caption of Fig. 7 are similar to those of the operational model (for the already assimilated channels) and combine errors from the background

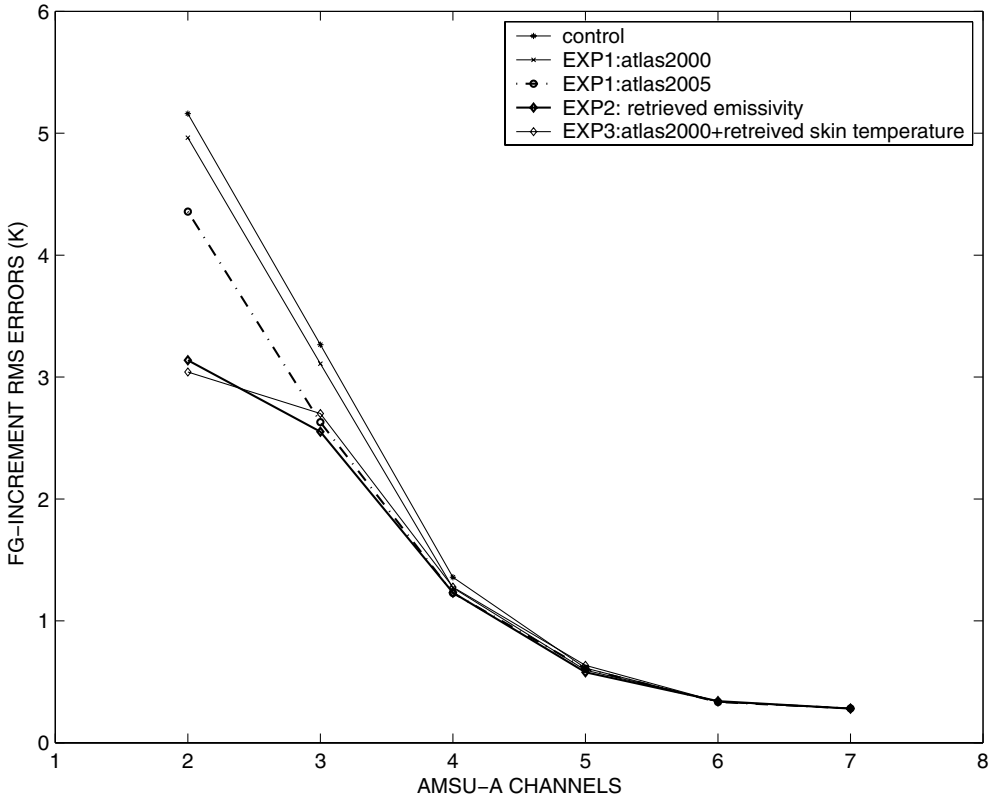

Figure 8. Mean fg-departure r.m.s. errors versus AMSU-A channels 2–7 calculated over the whole assimilation period and over all continents for the control experiment (solid line with asterisks), Exp1–Atlas2000 (solid line with crosses), Exp1–Atlas2005 (dotted line with circles), Exp2 (bold line with solid diamonds), and Exp3 (solid line with open diamonds).

and the observations. In the operational system, these thresholds are not the only condition for selecting channels to be assimilated. Other conditions have also to be satisfied, formulated in terms of surface type (sea, land, ice, etc.), orography, air mass, cloudiness, etc. Results given in Fig. 7 show that updating the surface scheme globally improves the statistics of fg-departures. However, for a given channel, the impact of each surface configuration is different. For AMSU-A channel 2 (31.4 GHz), Exp1–Atlas2005, Exp2 and Exp3 seem to give the best results. The bias and variability of fg-departures are reduced. We see an increase of the number of admissible observations with respect to the control while using the land configurations 2 and 3. For Exp1, better results are obtained using an atlas from year 2005 than from year 2000. Good results are also obtained for the remaining AMSU-A channels but are different for each experiment. For AMSU-A channel 3, the bias and variability are improved and the observation number increases when the surface configuration is changed. Similar conclusions are reached for AMSU-A sounding channels except for channels 6 and 7, for which we note a slight decrease in the number of observations with the third experiment. Biases and standard deviations are also improved for AMSU-B channel 2 compared with the control experiment. The increase of the number of admissible observations with respect to the

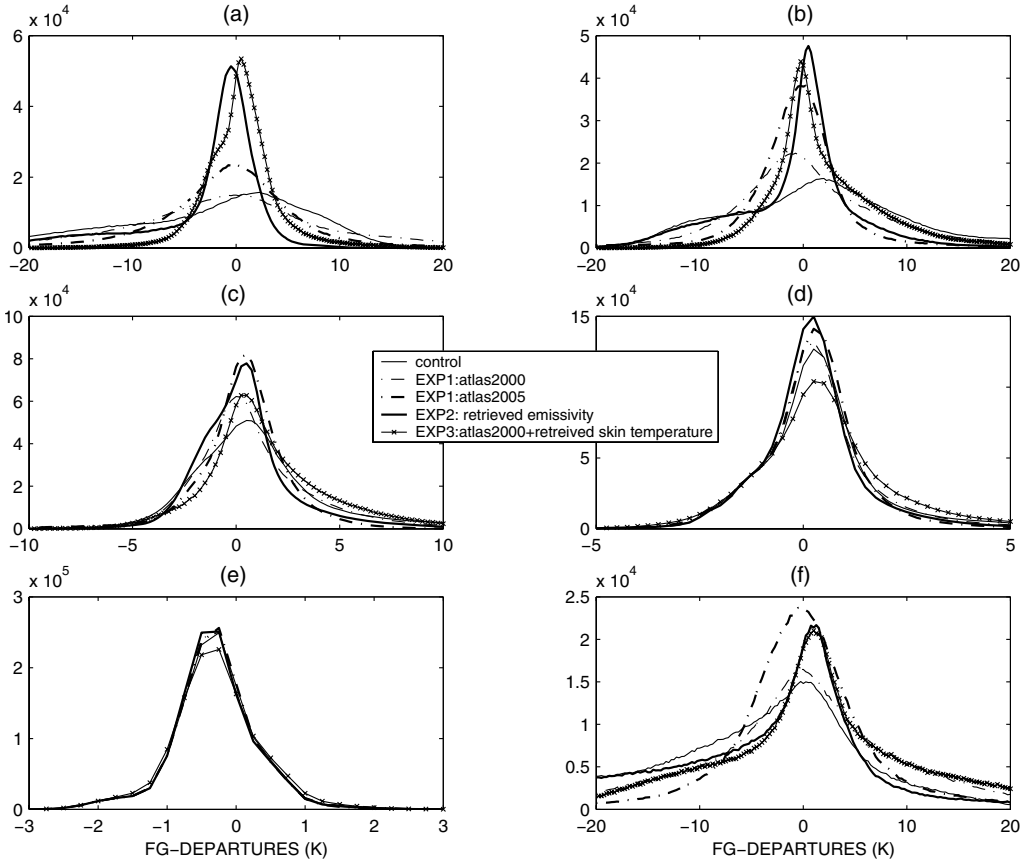

Figure 9. Histograms of fg-departure obtained using five assimilation experiments and for AMSU-A channels (a) 2, (b) 3, (c) 4, (d) 5, (e) 6, and (f) 15. Results from the control experiment, Exp1–Atlas2000, Exp1–Atlas2005, Exp2, and Exp3 are shown as solid, dash-dotted, bold dash-dotted, bold solid, solid with cross, respectively.

control for this channel is close to 140% for Exp2 and Exp3 and near 80% for Exp1–Atlas2005. The impacts are less important for AMSU-B sounding channels because they are less sensitive to the surface.

Figure 8 shows fg-departure r.m.s. error obtained globally over the whole experiment period, for AMSU-A channels 2 to 7. Significant improvement of the fg-departure r.m.s. error for surface channels is obtained when the land-surface configuration is modified. The best results are obtained with the second and third experiments. A smaller fg-increment r.m.s. error improvement is noticed for sounding channels. This was expected because these channels are less sensitive to the surface. Figure 9 completes this analysis by presenting fg-departure histograms for six AMSU-A channels. The histogram comparisons indicate that Exp1–Atlas2005, Exp2 and Exp3 show better statistics (mean, st.dev. values), with an increasing number of admissible observations (i.e. observations that could pass the quality-check step).

Similar results were obtained for AMSU-B channels (Fig. 10); the fg-departure statistics (mean, st.dev.) are improved and the number of admissible observations is increased with updated land-surface configurations.

However, Exp3 depends highly on the accuracy of the mean emissivity atlases in use and thus accumulates errors coming from emissivity and skin temperature

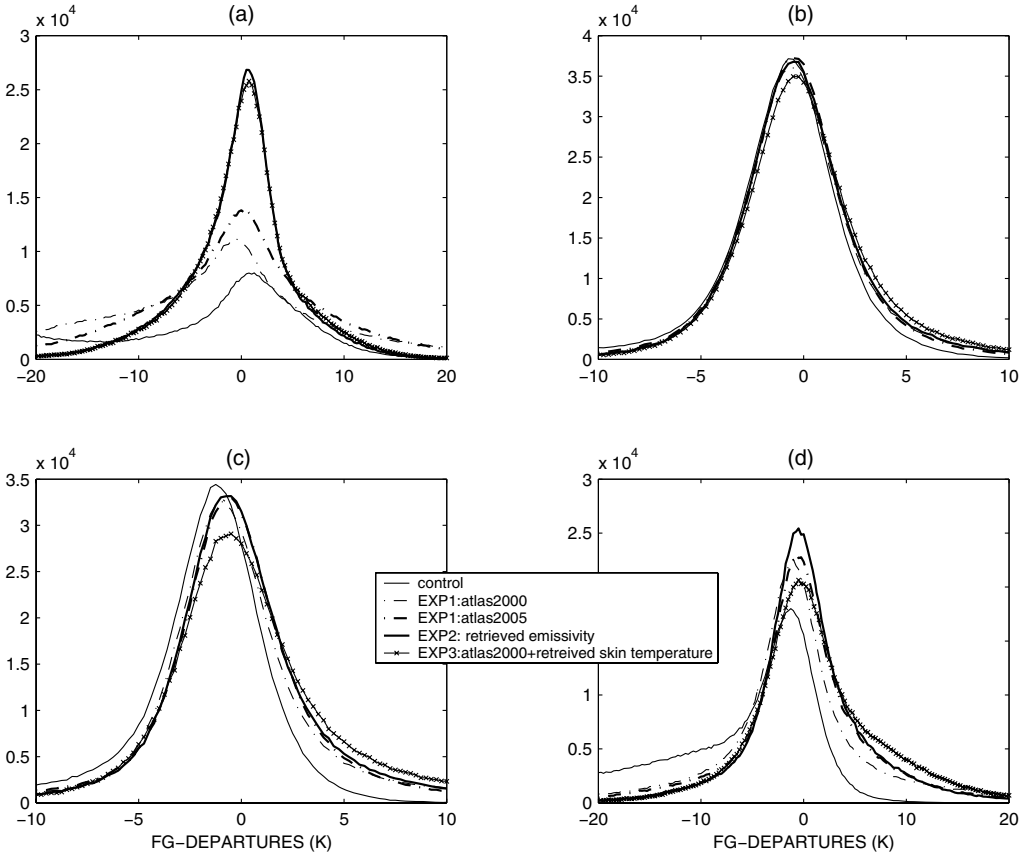

Figure 10. As Fig. 9, but for AMSU-B channels (a) 2, (b) 5, (c) 4, and (d) 3.

uncertainties. Exp1 may also be affected by errors in the emissivity atlas. Moreover, for this experiment, we use near-nadir emissivities. Consequently, the angular variation of the emissivity is not accounted for. For experiments with dynamic computations (emissivity or skin temperature), the angular variation of the emissivity as well as surface conditions (rain-induced soil moisture, vegetation change, etc.) are indirectly accounted for.

Figure 11 shows AMSU-A channel 3 fg-departure maps obtained over the (20°W–60°E; 0°–40°N) region. This figure illustrates some positive fg-departure biases for Exp1–Atlas2000 (Fig. 11(b)) probably caused by biases in the mean emissivity atlas. Indeed, an underestimation of the emissivity (due to rain-induced soil moisture effect, for example) could produce positive fg-departure biases. For the other experiments (Figs. 11(c)–(e)) the results are rather satisfactory. A small bias is noted for Exp2 results and could be explained by the fact that emissivities at 23.8 GHz may not be adapted for the 50 GHz channel. A frequency-dependent parametrization could probably reduce this effect. For Exp3, fg-departure biases may be caused by a combined effect of errors in the retrieved skin temperature and in emissivity estimates.

Additional fg-departure computations have been performed using Exp2 for 19 days in July 2005 and compared to the control (not shown). This comparison confirms the clear benefit of using the second land configuration for channels which receive a

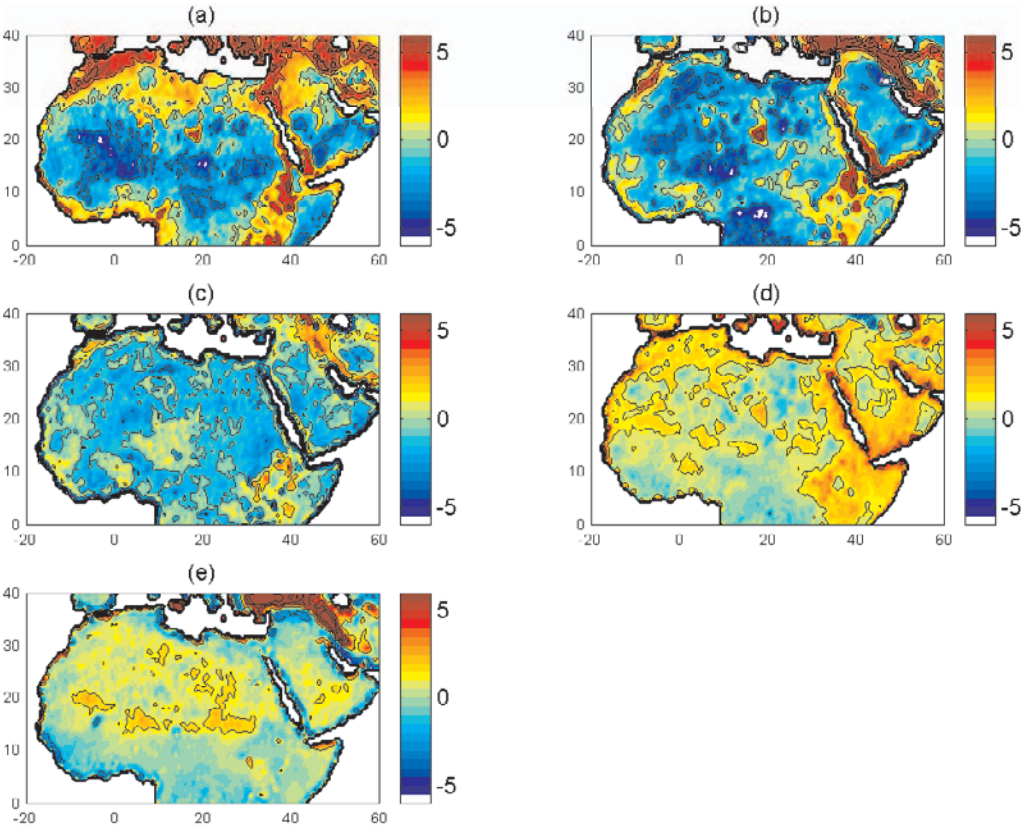

Figure 11. Mean fg-departures (colour shading, K) at 50 GHz (AMSU-A channel 3) averaged over the whole experiment period, obtained using 5 assimilation experiments: (a) the control, (b) Exp1–Atlas2000, (c) Exp1–Atlas2005, (d) Exp2, and (e) Exp3.

contribution from the surface. Further comparisons of both land schemes show that fg-departure r.m.s. errors are stable from one day to another for both experiments. We notice an fg-departure r.m.s. error improvement (with respect to the control) of around 53%, 29% and 12% for AMSU-A channels 2, 3, and 4 respectively while using the second surface scheme. The fg-departure r.m.s. error is also improved for the other AMSU-A channels.

Exp3 suffers from many limitations but has a great potential to characterize both land-surface emissivity and surface temperature. To overcome some of these limitations and in the framework of operational assimilation, emissivities can be carefully estimated using the latest archived month of AMSU data in order to produce updated mean emissivity atlases. Special care should be taken in order to avoid emissivity atlas contamination by clouds, rain and atmospheric errors. Moreover, skin temperature computation can be achieved only for very transmissive situations (here, the skin temperature is calculated if the atmospheric transmission is greater than 0.5) in order to limit skin temperature errors. In fact, with low atmospheric transmissions the retrieved skin temperatures are rather lower because of lower sensitivity to the surface. Exp1 could be improved by selecting a near-nadir emissivity atlas as carefully as possible. We note that better results are obtained when using an emissivity atlas close to the experiment period. Moreover, the emissivity atlas could be used with the addition of an emissivity

parametrization (Karbou 2005) in order to take into account the emissivity variation with the observation angle. Ongoing studies test the improvements described above to make better use of the new surface schemes.

It is important to note that AMSU-A and -B fg-departure histograms (Figs. 9 and 10) show that additional channels could pass the quality-check step over land if an adequate land-surface configuration is chosen. This is the case with AMSU-A channels 2, 3, 4, and 15 and also AMSU-B channel 2 when using the land configurations 1 (with Atlas2005), 2 and 3. Ongoing studies attempt to assimilate progressively these channels over land within the French 4D-Var system.

Results from the four experiments are further evaluated by calculating the differences between observed and simulated radiance with the analysed fields (called 'an-departures' hereafter). As before, no bias corrections have been applied for these comparisons. The an-departures are then compared with the fg-departures for AMSU channels that are assimilated operationally. The comparisons have been performed globally for all experiments, for AMSU-A channels 5–6 and for AMSU-B channels 3–4 (not shown). As expected, the an-increments are improved when compared to the fg-departures; once AMSU observations are assimilated, the analysis should be closer to the observations than the background. For AMSU-A channels, the an-departure mean improvement is more noticeable when the surface configuration is updated. For AMSU-B channels, the an-departure standard deviations are improved when compared to the fg-departures for all experiments.

The histograms of the analysed surface temperatures from the different experiments (not shown) show rather different surface temperature distributions. Within the 4D-Var system, the surface temperature analysis is performed independently from the atmospheric fields but uses air temperature background information from the nearest level to the surface. From one assimilation experiment to another, atmospheric temperature analyses and forecasts are modified which could imply significant changes for the analysed surface temperatures.

5. Conclusions

Depending on surface type and observation frequency, the 4D-Var operational surface scheme (at Météo-France) uses Grody (1988) or Weng *et al.* (2001) models to estimate the emissivity. In this study, three land-surface configurations are investigated, with the goal of extending the use of AMSU observations to channels that are sensitive to the surface. The first land configuration uses a monthly mean estimated land emissivity atlas using February 2000 AMSU-A and -B near-nadir observations at 23.8, 31.4, 50.3, 89, and 150 GHz. This land configuration was also used with a mean emissivity atlas derived using the first 20 days of March 2005. Within the second land scheme, dynamic land emissivity calculations are performed at 23.8 GHz (for AMSU-A processing) and at 89 GHz (for AMSU-B processing). These two channels are discarded from any other calculation or diagnostic to ensure the same information is not used twice. The emissivities thus obtained are assigned to the other AMSU-A or AMSU-B channels. The third land scheme is based on the first one with the addition of dynamic skin temperature estimation at 23.8 GHz (for AMSU-A processing) and at 89 GHz (for AMSU-B processing). These two channels are discarded from any other calculation or diagnostic. The calculated skin temperature is used as a guess for the remaining channels.

These land configurations have been applied within the French 4D-Var system over a two-week period and their results have been compared with those obtained using the

operational system. All land schemes have been evaluated by examining the performances of the 4D-Var observation operator prior to the assimilation. The performances of the observation operator have been examined using two diagnostics: (a) observation departure from first guess and (b) number of observations that could be used. The results of comparison show a significant improvement in the fg-departure statistics (mean, st.dev.) when the surface is updated with the new surface schemes. The results are different from one experiment to another. With Exp2 and Exp3, we note an increase of up to 140% in the number of observations that pass the quality-control check for AMSU-B channel 2 with respect to the control experiment. However, Exp2 gives good and geographically homogeneous results for this channel for both fg-departure r.m.s. errors and for the amount of admissible data. Moreover, this experiment does not need any emissivity atlas but only forecast fields. Exp3 has great potential to characterize both land-surface emissivity and skin temperature but depends on the accuracy of the mean emissivity atlas used. Results of Exp1 are best when using an emissivity atlas close to the experiment period. Results obtained at 89 GHz (AMSU-A channel 15) using Exp1 appear better than those obtained with the other land schemes in terms of 'observation departure from guess' distribution.

As a conclusion, the study indicates that additional AMSU-A and AMSU-B channels could indeed be assimilated, provided an adequate land configuration was chosen. AMSU-A channels 2–4 and 15 as well as AMSU-B channel 2 present satisfactory statistics that could allow their use in the 4D-Var system. However, if an experiment allows the use of a greater number of observations, it does not necessarily improve the forecast skill. The sensitivity studies conducted in this paper are not sufficient to assess the quality of each land scheme. Therefore, general conclusions concerning the performances of each land scheme are hard to draw. In particular, additional studies are needed to help to identify the best land scheme for our 4D-Var system.

The impact of microwave skin temperature and emissivity errors (2% in emissivity and 5 K in skin temperature) on T_b simulations, at surface and sounding frequencies, has also been studied. This impact varies with frequency, and with surface and atmospheric conditions and should not be ignored even for sounding channels.

More in-depth studies are needed in order to evaluate more precisely the impact of each land configuration on both surface and atmospheric fields. However, such studies cannot be undertaken unless some well-identified problems are solved. Firstly, bias-correction coefficients as well as observation and background-error statistics should be updated so as to include surface channels. In this context, efforts will focus on the estimation of bias-correction coefficients that are appropriate for both land and ocean surfaces and for all available AMSU sensors. Secondly, additional tests should be performed in order to choose a new land configuration that gives the best results for analysis fields and forecast skill when surface channels are assimilated. Improved versions of experiments 1, 2 and 3 are now being tested over longer periods in assimilation mode and results will be reported in a subsequent paper. The proposed land configurations could be applied to other microwave sensors such as SSM/I, SSMI/S, among others.

ACKNOWLEDGEMENTS

The authors wish to thank Jean Maziejewski for his help in revising the manuscript. The authors are very grateful to three anonymous reviewers as well as to the associate editor for detailed and helpful comments about the manuscript. They also appreciate interesting discussions with Laurence Eymard and Catherine Prigent. F. Karbou acknowledges financial support from the Centre National d'Etudes Spatiales (CNES).

REFERENCES

Aires, F., Prigent, C., Rossow, W. B. and Rothstein, M. 2001 A new neural network approach including first guess for retrieval of atmospheric water vapour, cloud liquid water path, surface temperature, and emissivities over land from satellite microwave observations. *J. Geophys. Res.*, **106,** 14887–14907

Basist, A., Grody, N. C., Peterson, T. C. and Williams, C. N. 1998 Using the Special Sensor Microwave/Imager to monitor land surface temperatures, wetness, and snow cover. *J. Atmos. Sci.*, **37,** 888–911

Calvet, J.-C., Wigneron, J. P., Chanzy, A., Raju, S. and Laguerre, L. 1995 Microwave dielectric proprieties of a silt-loam at high frequencies. *IEEE Trans. Geosci. Remote Sensing*, **33,** 634–642

Choudhury, B. J. 1993 Reflectivities of selected land surface types at 19 and 37 GHz from SSM/I observations. *Remote Sens. Environ.*, **46,** 1–17

Courtier, P., Thépaut, J. N. and Hollingsworth, A. 1994 A strategy for operational implementation of 4D-Var using an incremental approach. *Q. J. R. Meteorol. Soc.*, **114,** 1321–1387

Deblonde, G. and English, S. J. 2000 'Evaluation of fastem and fastem2 fast microwave oceanic surface emissivity model'. Pp. 67–78 in Proceedings of the 11th International ATOVS study conference, Budapest, Hungary

English, S. J. 1999 Estimation of temperature and humidity profile information from microwave radiances over different surface types. *J. Appl. Meteorol.*, **38,** 1526–1541

Eyre, J. R. 1991 'A fast radiative transfer model for satellite sounding systems'. Tech. Memo. 176, ECMWF, Reading, UK

Felde, G. W. and Pickle, J. D. 1995 Retrieval of 91 and 150 GHz Earth surface emissivities. *J. Geophys. Res.*, **100,** D10, 20855–20866

Goodrum, G., Kidwell, K. B. and Winston, W. 2000 'NOAA KLM user's guide'. NOAA/NESDIS/NCDC, Washington DC, USA. http://www2.ncdc.noaa.gov/docs/klm/index.htm

Grody, N. C. 1988 Surface identification using satellite microwave radiometers. *IEEE Trans. Geosci. Remote Sensing*, **26,** 850–859

Guillou, C., Ellison, W., Eymard, L., Lamkaouci, K., Prigent, C., Delbos, G., Balana, G. and Boukabara, S. A. 1998 Impact of new permittivity measurements on sea surface emissivity modelling in microwaves. *Radio Science*, **33,** 649–667

Guissard, A. and Sobieski, P. 1987 An approximate model for the microwave brightness temperature of the sea. *Int. J. Remote Sensing*, **8,** 1607–1627

Hewison, T. J. 2001 Airborne measurements of forest and agricultural land surface emissivity at millimetre wavelengths. *IEEE Trans. Geosci. Remote Sensing*, **39,** 2393-2400

Hewison, T. J. and English, S. J. 1999 Airborne retrieval of snow and ice surface emissivity at millimetre wavelengths. *IEEE Trans. Geosci. Remote Sensing*, **37,** 1871–1879

Isaacs, R. G., Jin, Y.-Q., Worsham, R. D., Deblonde, G. and Falcone, V. J. 1989 The RADTRAN microwave surface emission models. *IEEE Trans. Geosci. Remote Sensing*, **27,** 433–440

Janiskova, M., Thépaut, J. N. and Geleyn, J. F. 1999 Simplified and regular physical parameterization for incremental four dimentional variational assimilation. *Mon. Weather Rev.*, **127,** 26–44

Jones, A. S. and Vonder Haar, T. H. 1997 Retrieval of microwave surface emittance over land using coincident microwave and infrared satellite measurements. *J. Geophys. Res.*, **102,** D12, 13609–13626

Karbou, F. 2005 Two microwave land emissivity parameterizations suitable for AMSU observations. *IEEE Trans. Geosci. Remote Sensing*, **43**(8)**,** 1788–1795

Karbou, F. and Prigent, C. 2005 Calculation of microwave land surface emissivities from satellite observations: validity of the specular approximation over snow-free surfaces. *IEEE Trans. Geosci. Remote Sensing Letts.*, **2**(3)**,** 311–314

Karbou, F., Prigent, C., Eymard, L. and Pardo, J. 2005a Microwave land emissivity calculations using AMSU-A and AMSU-B measurements. *IEEE Trans. Geosci. Remote Sensing*, **43**(5)**,** 948–959

Karbou, F., Aires, F., Prigent, C. and Eymard, L. 2005b Potential of Advanced Microwave Sounding Unit-A (AMSU-A) and AMSU-B measurements for temperature and humidity sounding over land. *J. Geophys. Res.*, **110,** D07109, doi: 10.1029/2004JD005318

MacFarland, J. M., Miller, R. L. and Neale, C. M. U. 1990 Land surface temperature derived from the SSM/I passive microwave brightness temperatures. *IEEE Trans. Geosci. Remote Sensing*, **28,** 839–843

Matricardi, M., Chevallier, F., Kelly, G. and Thépaut, J. N. 2004 An improved general fast radiative transfer model for the assimilation of radiance observations. *Q. J. R. Meteorol. Soc.*, **130,** 153–173

Mätzler, C. 1990 Seasonal evolution of microwave radiation from an oat field. *Remote Sens. Environ.*, **31,** 161–173

1994 Passive microwave signatures of landscapes in winter. *Meteorol. Atmos. Phys.*, **54,** 241–260

2005 On the determination of surface emissivity from satellite observations, IEEE Geoscience and remote sensing letters. *IEEE Geosci. Remote Sensing Letts.*, **2**(2)**,** 160–163

Morland, J. C., Grimes, D. I. F., Dugdale, G. and Hewison, T. J. 2000 The estimation of land surface emissivities at 24 to 157 GHz using remotely sensed aircraft data. *Remote Sensing Environ.*, **73,** 3323–3336

Morland, J. C., Grimes, D. I. F. and Hewison, T. J. 2001 Satellite observations of the microwave emissivity of a semi-arid land surface. *Remote Sensing Environ.*, **77,** 2149–2164

Pardo, J. R., Cernicharo, J. and Serabyn, E. 2001 Atmospheric Transmission at Microwave (ATM): an improved model for millimetre/submillimetre applications. *IEEE Trans. Antenn. Propag.*, **49**(12)**,** 1683–1694

Prigent, C. and Abba, P. 1990 Sea surface equivalent brightness temperature at millimeter wavelength. *Annales Geophysicae*, **8,** 627–634

Prigent, C., Rossow, W. B. and Matthews, E. 1997 Microwave land surface emissivities estimated from SSM/I observations. *J. Geophys. Res.*, **102,** 21867–21890

1998 Global maps of microwave land surface emissivities: potential for land surface characterization. *Radio Sci.*, **33,** 745–751

Prigent, C., Wigneron, J. P., Rossow, B. and Pardo, J. R. 2000 Frequency and angular variations of land surface microwave emissivities: can we estimate SSM/T and AMSU emissivities from SSM/I emissivities? *IEEE Trans. Geosci. Remote Sensing*, **38**(5)**,** 2373–2386

Prigent, C., Aires, F., and Rossow, B. 2003 Land surface skin temperatures from a combined analysis of microwave and infrared satellite observations for an all-weather evaluation of the differences between air and skin temperatures *J. Geophys. Res.*, **108,** D10, 4310, doi: 10.1029/2002JD002301

Prigent, C., Chevallier, F., Karbou, F., Bauer, P. and Kelly, G. 2005 AMSU-A surface emissivities for numerical weather prediction assimilation schemes. *J. Appl. Meteorol.*, **44,** 416–426

Rabier, F., Järvinen, H., Klinker, E., Mahfouf, J. F. and Simmons, A. 2000 The ECMWF operational implementation of four dimentional variational assimilation. I: Experimental results with simplified physics. *Q. J. R. Meteorol. Soc.*, **126,** 1143–1170

Rosenkranz, P. W. and Staelin, D. H. 1972 Microwave emissivity of ocean foam and its effect on nadiral radiometric measurements. *J. Geophys. Res.*, **77,** 6528–6538

Rossow, W. B. and Garder, L. C. 1993a Cloud detection using satellite measurements of infrared and visible radiances for ISCCP. *J. Climate*, **6,** 2341–2369

1993b Validation of ISCCP Cloud detection. *J. Climate*, **6,** 2370–2393

Rossow, W. B. and Schiffer, R. A. 1991 ISCCP cloud data products. *Bull. Am. Meteorol. Soc.*, **72,** 2–20

Saunders, R. W., Matricardi, M. and Brunel, P. 1999 An improved fast radiative transfer model for assimilation of satellite radiance observations. *Q. J. R. Meteorol. Soc.*, **125,** 1407–1425

Simmons, A. J. and Gibson, J. K. 2000 'The ERA-40 project plan'. ERA-40 project report No. 1, ECMWF, Reading, UK

Trigo, I. F. and Viterbo, P. 2003 A comparison between observations and the ECMWF model. *J. Appl. Meteorol.*, **42,** 1463–1479

Uppala, S. M., Kållberg, P. W., Simmons, A. J., Andrae, U., Da Costa Bechtold, V., Fiorino, M., Gibson, J. K., Haseler, J., Hernandez, A., Kelly, G. A., Li, X., Onogi, K., Saarinen, S., Sokka, N., Allan, R. P., Andersson, E., Arpe, K., Balmaseda, M. A., Beljaars, A. C. M., Van de Berg, L., Bidlot, J., Bormann, N., Caires, S., Chevallier, F., Dethof, A., Dragosavac, M., Fisher, M., Fuentes, M., Hagemann, S., Hólm, E., Hoskins, B. J., Isaksen, L., Janssen, P. A. E. M., Jenne, R., McNally, A. P., Mahfouf, J.-F., Morcrette, J.-J., Rayner, N. A., Saunders, R. W., Simon, P., Sterl, A., Trenberth, K. E., Untch, D., Vasiljevic, D., Viterbo, P. and Woollen, J. 2005 The ERA-40 re-analysis. *Q. J. R. Meteorol. Soc.*, **131,** 2961–3012

Veersé, F. and Thépaut, J. N. 1998 Multiple truncation incremental approach for four-dimensional variational data assimilation. *Q. J. R. Meteorol. Soc.*, **124,** 1889–1908

Weng, F., Yan, B. and Grody, N. 2001 A microwave land emissivity model. *J. Geophys. Res.*, **106,** D17, 20115–20123

Wentz, F. 1975 A two-scale scattering model for foam-free sea microwave brightness temperatures. *J. Geophys. Res.*, **80,** 3441–3446

Wigneron, J.-P., Guyon, D., Calvet, J.-C., Courrier, G. and Bruiguier, N. 1997 Monitoring coniferous forest characteristics using a multifrequency microwave radiometry. *Remote Sensing Environ.*, **60,** 299–310

Williams, C. N., Basist, A., Peterson, T. C. and Grody, N. 2000 Calibration and verification of land surface temperature anomalies derived from the SSM/I. *Bull. Am. Meteorol. Soc.*, **81,** 2141–2156